COBEM 2023 27TH INTERNATIONAL CONGRESS OF MECHANICAL ENGENEERING

ABCM Brazilian Society of Mechanical Sciences and Engineering
27th ABCM International Congress of Mechanical Engineering
December 04-08, 2023, Florianópolis-SC, Brazil

# COB-2023-1594 Numerical Investigation of Water Alternating Gas Injection Ratios on Multiphase Flow in Porous Media for Enhanced Oil Recovery

**Vinícius Rafael de Freitas**
**Adriano Rosa**
**Eugênio Fortaleza**
Department of Mechanical Engineering, University of Brasília, Brasília, Federal District, Brazil
vinicius_r_freitas@hotmail.com
aprosa@unb.br
efortaleza@unb.br

**Rafael Valladares**
Repsol Sinopec Brasil, Pesquisa e Desenvolvimento, Rio de Janeiro, RJ, Brazil
rafael.valladares@repsolsinopec.com

***Abstract.*** *Enhanced oil recovery techniques are widely used in real oil fields, with Water Alternating Gas (WAG) injection being one of the most employed methods due to its simplicity and low-cost application. In addition to mitigating the Saffman-Taylor instability, WAG injection can lead to better oil recovery, matching better mobility control and allowing previously trapped zones to be swept through better microscopic displacement. In this work, we investigate the effects of different WAG ratios on multiphase flow in porous media, with a focus on enhanced oil recovery. Our objective is to optimize oil production by gaining a better understanding on the factors that impact oil production. We use OpenFOAM, an open-source CFD software, to numerically simulate the flow of oil, water, and gas through a porous media, using a finite-volume discretization methodology. We examine a range of different injection schedules, including classic injection schemes, such as gas flooding, water flooding, and common WAG ratios (1:1, 1:4, and 4:1) and non-traditional WAG ratios, to study their effects on oil production total, flow pattern, and investigate the formation of viscous fingering at the interface between the phases. Our findings indicate that the gas phase exhibits a propensity to explore specific regions within the reservoir, while the water phase efficiently displaces the remaining oil from these areas. Therefore, the combination of these effects can lead to optimal oil production.*

***Keywords:*** *WAG, Oil Reservoir, EOR, Multiphase Flow, OpenFOAM.*

## 1. INTRODUCTION

Enhanced Oil Recovery (EOR) is an area of great importance in the oil and gas industry, as a large amount of oil remains trapped in reservoirs after primary and secondary production. For a typical oilfield, the average recovery factor is approximately $40\%$ (Afzali *et al.*, 2018). EOR techniques have the potential to recover an incremental percentage of oil. Such improvement occurs through modification of fluids properties in the reservoir, or fluid/rock interaction, to create more favorable conditions for oil recovery.

Among EOR techniques, Water Alternating Gas (WAG) is one of the most used and consolidated due to its simplicity and low application cost, in addition to other benefits it offers to the oil recovery process. Skauge and Stensen (2003) reviewed 59 real WAG fields and revealed that, in the cases studied, the average oil recovery increases more than $10\%$ in relation to the Originally Oil In Place in all WAG cases. Other studies show an increase of the same order of magnitude, being $14\%$ in the Immiscible WAG (IWAG) study by Mousavi Mirkalaei *et al.* (2011) and $9.5\%$ in the study by Ramachandran *et al.* (2010).

WAG combines the improved displacement efficiency of the gas flood with a macroscopic sweep enhanced by the water injection (Christensen *et al.*, 2001), making previously trapped zones recoverable, in addition to mitigating fluid front instability (Saffman-Taylor instability or viscous fingering) (Afzali *et al.*, 2018). Christensen *et al.* (2001) show that the most popular WAG ratio found in oil fields is $1:1$, while Afzali *et al.* (2018) shows that another popular WAG ratios are $1:4$ and $4:1$, as used in the works by Al-Shuraiqi (2005) and Christie *et al.* (1993).

Reservoir-scale simulations still have some limitations. To overcome these challenges, it is crucial to conduct pore-scale studies in order to improve our understanding of fluid flow in porous media and, consequently, enhance the efficiency of oil recovery techniques. This need becomes evident when we examine recent research focused on Pore-Scale Investigation for Enhancing Oil Recovery, as exemplified by the works of Ju *et al.* (2020), Iyi *et al.* (2021), Britto *et al.* (2020), Zhao and Wen (2017), and Zhu *et al.* (2017). Blunt *et al.* (2013) support this idea and states that pore-scale modeling has experienced significant advancement, evolving from a technique primarily focused on understanding displacement processes without commercial exploitation to becoming a widely utilized predictive tool in the oil industry.

Open-source Field Operation and Manipulation (OpenFOAM), a computational fluid dynamics software, has been widely used in modeling fluid flow in porous media (Ranaee *et al.*, 2020; Guédon *et al.*, 2019; Yu *et al.*, 2022; Raeini *et al.*, 2012; Menke *et al.*, 2015; Al-Khulaifi *et al.*, 2019), including advanced oil recovery applications. OpenFOAM's ability to handle complex geometries and the flexibility of open-source code make it an attractive choice for flow simulations in porous media. In particular, water-gas injection (WAG) modeling in oil reservoirs can be better explored using OpenFOAM due to the possibility of pore-scale analysis and easy visualization.

The present work aims to investigate the effects of different WAG ratios on multiphase flow in porous media, with a specific focus on oil recovery. Using numerical simulations based on OpenFOAM, this study aims to identify optimal injection ratios and improve our understanding of reservoir fluid dynamics. The goal is to integrate this knowledge to the optimization techniques previously explored and presented by our research group, as presented in the works of Fortaleza *et al.* (2020) and de Freitas *et al.* (2020). A variety of different injection schemes will be examined, including classic injection schemes such as gas flooding (GF) and water flooding (WF), common WAG ratios (1:1, 1:4, 4:1 and its intermediaries) as well as simultaneous WAG (SWAG), which consists in the simultaneous injection of water and gas. The investigation is focused on the effect of the injection scheme on oil production, pattern flow and the formation of viscous fingers at the interface between the phases. The results obtained in this study can offer valuable insights, contributing to the development of more efficient strategies for oil recovery.

## 2. Problem Formulation and Numerical Methodology

To explore the effects of various WAG ratios, we analyze the flow within a square domain measuring $L = 10\,mm$ in length, with a porosity of $47.94\%$. This domain is depicted in Figure 1. The porosity was achieved by including 25 circles of radius $R_1 = 0.7692\,mm$ and 12 circles of radius $R_2 = 0.3846\,mm$. The inlet and the outlet, located at opposite ends of the domain, have a width of $1\,mm$ each. All meshes in this work were generated with the aid of Gmesh software (Geuzaine and Remacle, 2009) and post-processing with Paraview software (Fabian *et al.*, 2011).

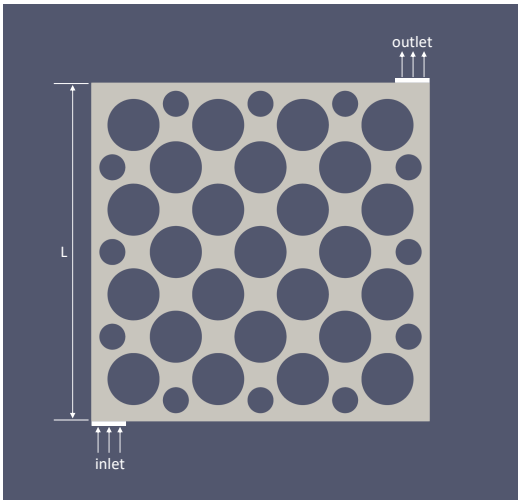


Figure 1: Schematic illustration of the problem geometry investigated in this work. The domain is represented as a square with a length denoted by $L$. The fluid enters the domain via the inlet and exits through the outlet.

The boundary condition adopted in the inlet is constant speed of $0.01\,m/s$. At the outlet, the adopted boundary condition was pressure of $0\,Pa$. Finally, the non-slip condition was considered for the walls. The domain is initially filled with oil, which is characterized by a density of $\rho = 940\,kg/m^3$ and a kinematic viscosity $\nu = 10.6 \times 10^{-6}\,m^2/s$. Water ($\rho = 1000\,kg/m^3$, $\nu = 1 \times 10^{-6}\,m^2/s$) and gas ($\rho = 1\,kg/m^3$, $\nu = 14.8 \times 10^{-6}\,m^2/s$) are injected in the domain through the inlet port. In this work, some simplifications were adopted: we consider an incompressible flow and the surface tension and the wettability are disregarded.

A variety of different injection schemes are examined in the simulations. The total time duration is fixed in 6 seconds. For WAG cases, only one complete cycle will be evaluated and will start with water injection. For WAG $1:1$, for example, water is injected continuously from zero to three seconds while, after that, gas is injected until the end to complete one entire WAG cycle.

The simulations in this study were conducted using the multiphaseInterFoam solver, from OpenFOAM 9, from The OpenFOAM Foundation. In this solver, the Finite Volume Method (FVM) is used in the discretization of the equations and the Volume of Fluid (VOF) method is used to solve the multiphase flow. The phase volume fraction is $\alpha_i$, where $i = 1$

for water, $i = 2$ for gas and $i = 3$ for oil. The fluid mixture density $\rho$ and viscosity $\mu$ are calculated as

$$\rho = \alpha_1\rho_1 + \alpha_2\rho_2 + \alpha_3\rho_3 \ , \tag{1}$$

$$\mu = \alpha_1\mu_1 + \alpha_2\mu_2 + \alpha_3\mu_3 \ , \tag{2}$$

with

$$\alpha_1 + \alpha_2 + \alpha_3 = 1 \ . \tag{3}$$

The mass conservation equation for each phase and the momentum equation are written as

$$\frac{\partial \alpha_i}{\partial t} + \frac{\partial \left(\alpha_i u_j\right)}{\partial x_j} = 0 \ , \tag{4}$$

$$\frac{\partial}{\partial t}\left(\rho u_i\right) + \frac{\partial}{\partial x_j}\left(\rho u_i u_j\right) = -\frac{\partial p}{\partial x_i} + \frac{\partial}{\partial x_i}\left[\mu\left(\frac{\partial u_j}{\partial x_i} + \frac{\partial u_i}{\partial x_j}\right)\right] \ , \tag{5}$$

respectively, where $p$ is the pressure and $u_i$ is the $i$-th component of the velocity vector.

In the simulations configurations, we have used the Euler method for time integration with a fixed time-step of $10^{-5}\,s$. The diffusive term is approximated by a second-order linear implementation, while we have used a second-order linear upwind method for the convective terms. We have used the PIMPLE scheme to handle the coupling between the pressure and velocity fields.

### 2.1 Mesh Convergence Test

The fluid domain was discretized in an unstructured triangular mesh with local refinement close to the inlet, to the outlet and around the grains. To study the dependence of the result on the mesh refinement, we investigated three different meshes, namely Mesh 1 (10200 cells), Mesh 2 (39432 cells) and Mesh 3 (155808 cells). Figure 2 shows the mesh details close to the inlet. Meshes 2 and 3 also have layers of quadrilateral cells close to the grains boundary.

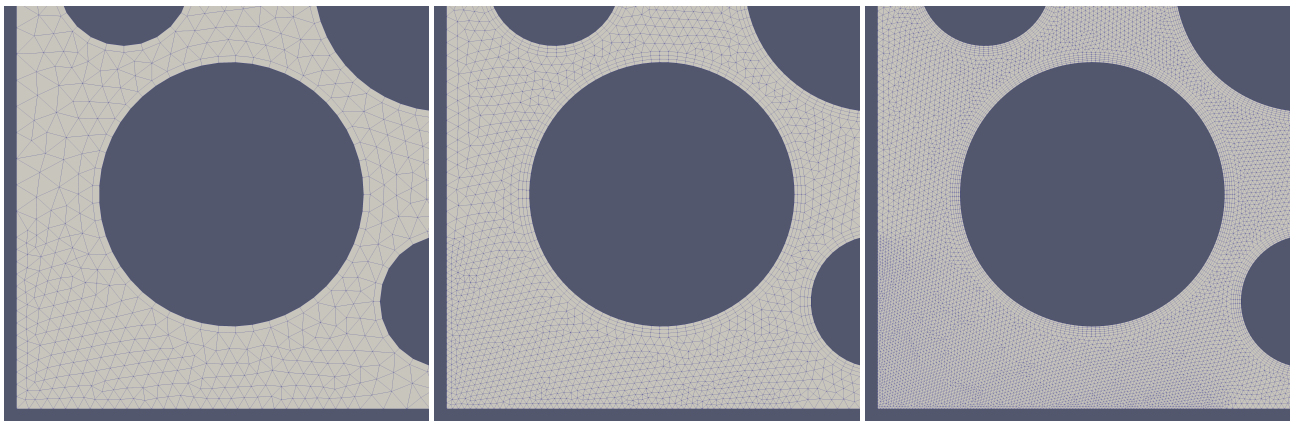

(a) Mesh 1 (b) Mesh 2 (c) Mesh 3

Figure 2: Mesh details at inlet.

To evaluate the results for the three meshes, water flooding (WF) and gas flooding (GF) simulations were performed, with a final simulation time of $t = 10\,s$. The evolution of the Oil Recovery Factor (ORF) over time is presented in Figure 3. Notably, the results for meshes 2 and 3 exhibit close proximity to each other. In the case of WF simulations, meshes 2 and 3 demonstrate similar behavior throughout the entire simulation duration. Conversely, for GF simulations, there are slight differences in results between $t = 1\,s$ and $t = 4\,s$, but they converge and remain consistent thereafter. Additionally, meshes 2 and 3 exhibit the same breakthrough time and yield similar overall ORF values at the end of the simulations.

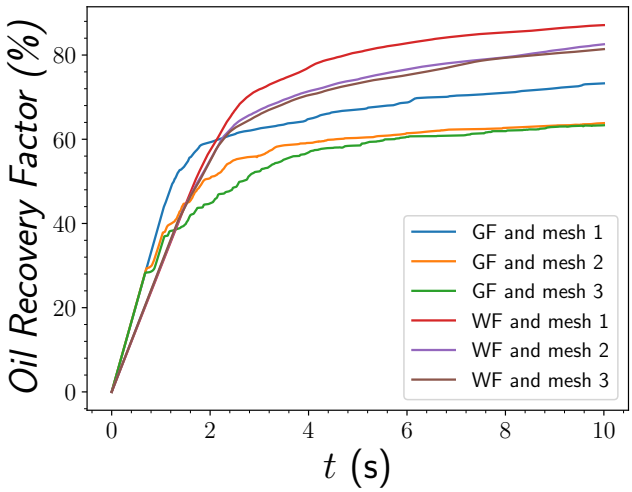


Figure 3: Oil Recovery Factor for different mesh refinement.

The plots in Figure 4 show the fluids saturation for the GF and WF cases. The results for mesh 1 are significantly different from those observed for meshes 2 and 3.

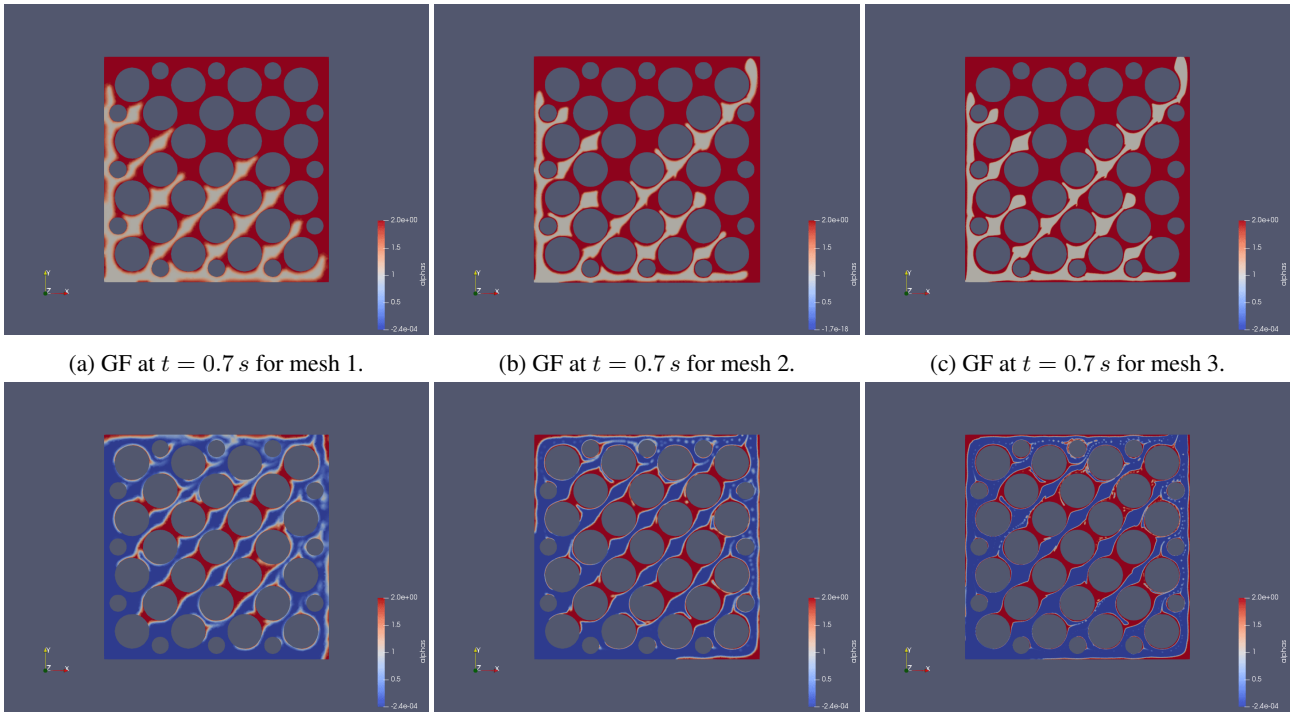

(a) GF at $t = 0.7\ s$ for mesh 1. (b) GF at $t = 0.7\ s$ for mesh 2. (c) GF at $t = 0.7\ s$ for mesh 3.

(d) WF at $t = 4.0\ s$ for mesh 1. (e) WF at $t = 4.0\ s$ for mesh 2. (f) WF at $t = 4.0\ s$ for mesh 3.

Figure 4: Snapshots of the simulation for GF and WF for in different meshes. The plots show the ternary saturation at $t = 0.7$ for GF and $t = 4.0$ for WF, with water shown in blue, gas in gray, and oil in red.

Based on these results, we have decided to use mesh 2 in the remaining simulations of this study. Mesh 2 has a smaller computational cost than mesh 3 and presents very similar results.

## 3. Results and Discussion

The results of different schedules of water and gas injections are presented in this section. All simulations were run until $t = 6\ s$ and WAG cases always start with water injection, proceeded by gas injection, completing one cycle.

The schedules of gas injection during the entire simulation (GF) and that of water only injection (WF) represent the limit scenarios in this study. Figures 5 and 6 show the results of the ternary saturation for these cases. The red color in the images represents the oil, while blue represents water and gray color indicates the presence of gas. Figures 5a and 5b depict the initial stage of gas injection and the moment just before the gas injected reaches the outlet (which is called

breakthrough), respectively. Notably, the gas flow predominantly follows a diagonal path connecting the inlet and outlet. Although the gas effectively displaces a significant portion of the oil surrounding the grains, a residual amount of oil remains in the vicinity of the reservoir walls.

Figure 5c depict the moment close to the end of the simulation, at $t = 5\,s$, respectively. It is evident that the gas front progresses along alternative pathways, bypassing the grains in nearly all regions. However, a significant quantity of oil remains adhered to the walls, indicating the gas's limited ability to displace it in these particular areas.

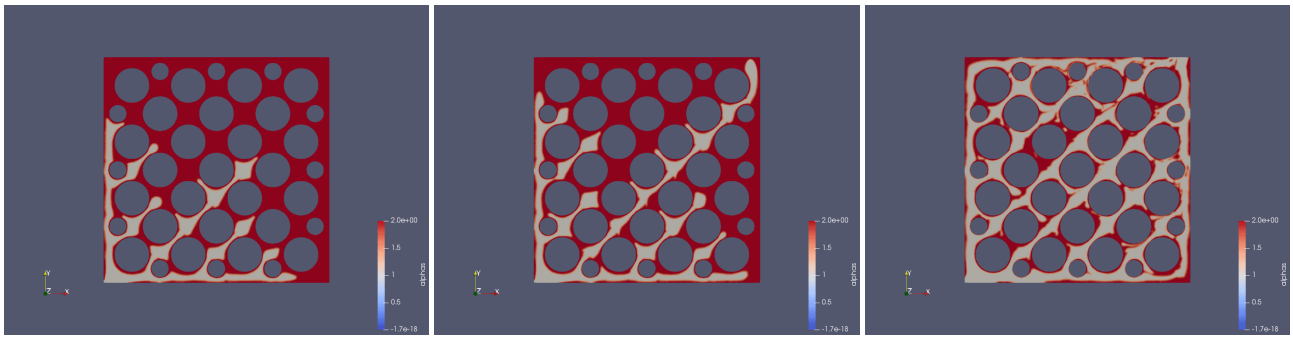

(a) Close to the start time, at $t = 0.5\,s$. (b) Before breakthrough, at $t = 0.7\,s$. (c) Close to the end time, at $t = 5.0\,s$.

Figure 5: Ternary saturation at different times during the simulation for the gas flood (GF) case. The gas phase volume fraction is depicted in gray, and the oil phase is represented in red.

The WF case, on the other hand, exhibits a distinct behavior. Water demonstrates a more homogeneous advancement in all directions, as illustrated in Figures 6a and 6b. While it also leaves behind some oil, the remaining oil saturation is considerably lower compared to the GF case. Another noteworthy distinction lies in the advancement rate of the displacement front. The breakthrough of the GF case, shown in Figure 5b, occurs at $t = 0.7\,s$, while the same breakthrough in the WF case (Figure 6b) is delayed until $t = 1.4\,s$. This discrepancy stems from the viscosity contrast, resulting in a faster displacement front in the GF case in comparison to the WF case. Figure 6c provide evidence supporting the notion that water displacement leaves less residual oil. This image reveal that the region near the inlet is almost entirely flooded with water, with minimal oil remaining around the grains. However, in the central regions of the reservoir, except along the main diagonal, water is less effective in sweeping the oil.

The ORF for both the WF and GF cases is presented in Figure 3 (mesh 2). Initially, the gas ORF is higher, indicating a rapid production of oil due to its lower viscosity. However, after approximately $1.2\,s$, the situation reverses, and water consistently achieves a higher ORF at all subsequent time points until the end of the simulation. While the gas exhibits a swift oil production, it also leaves behind a significant amount of residual oil. On the other hand, water advances more slowly but effectively sweeps away a larger portion of the oil.

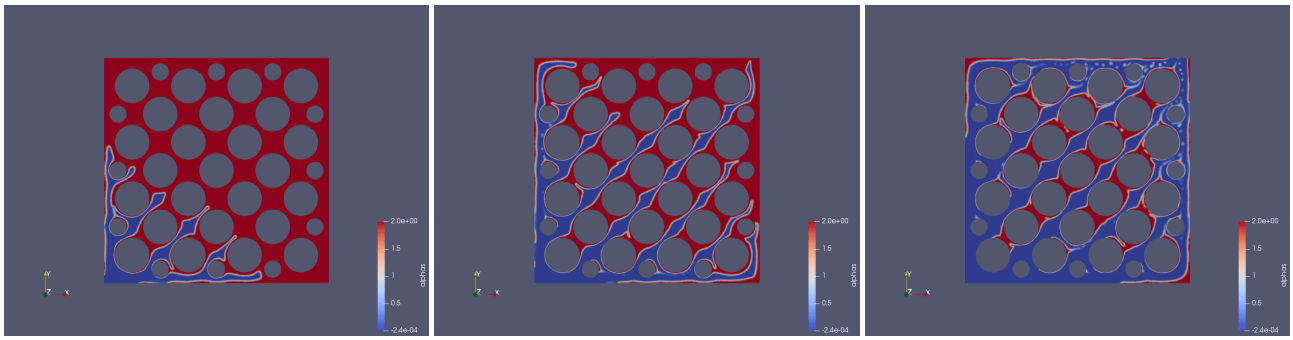

(a) Close to the start time, at $t = 0.5\,s$. (b) Before breakthrough, at $t = 1.4\,s$. (c) Close to the end time, at $t = 5.0\,s$.

Figure 6: Ternary saturation at different times during the simulation for the water flooding (WF) case. The water phase volume fraction is depicted in blue, and the oil phase is represented in red.

After investigating pure water and gas injections, we proceed with the investigation of mixed injections, specifically Water Alternating Gas (WAG) injection. Figure 7 illustrates the WAG 1:1 ternary saturation at $t = 4\,s$ (a), $t = 5\,s$ (b) and $t = 6\,s$ (c). The WAG 1:1 simulation corresponds to a water injection between $t = 0\,s$ and $t = 3\,s$ and a gas injection between $t = 3\,s$ and $t = 6\,s$. In this way, the WAG 1:1 simulation is the same as the WF simulation, shown in Figure

6, until $t = 3\,s$. In Figure 7a, it can be observed that the gas flows within the water phase. This can be attributed to the formation of a preferential pathway facilitated by the water, allowing for the easier flow of another fluid through this pathway. Figures 7b and 7c reveal that, even at more advanced time points, the gas does not seek new pathways, and the oil trapped primarily in the central region of the reservoir remains untouched by the injected fluids. Additionally, the difference between Figures 7b and 7c is minimal, suggesting that during this time interval, the fluids produced from the reservoir were primarily the same as those injected. We also investigated other WAG injection schedules, including 2:1, 3:1, 4:1, 1:2, 1:3, and 1:4. The results of these simulations are discussed in detail later in the text.

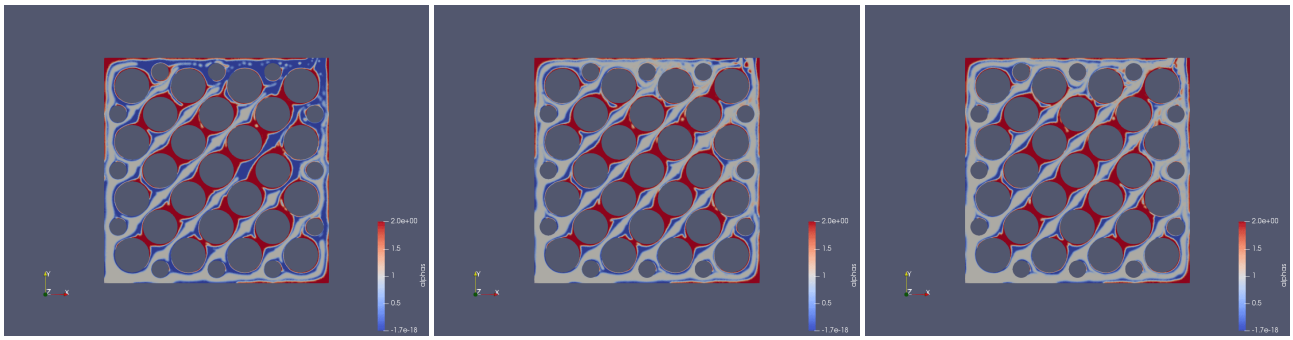

(a) $t = 4.0\,s$. (b) $t = 5.0\,s$. (c) $t = 6.0\,s$.

Figure 7: Ternary saturation at different times during the simulation for the Water Alternating Gas 1:1 (WAG 1:1) case. The water phase volume fraction is depicted in blue, the gas phase in gray and the oil phase is represented in red.

After conducting the WAG simulations, we turn our attention to the simultaneous injection case, where water and gas phases are injected simultaneously and in equal proportions, each accounting for $50\%$ of the mixture. Figure 8 illustrates the ternary saturation for SWAG at $t = 0.5\,s$, $t = 0.85\,s$ and $t = 5\,s$.

Figures 8a and 8b depict an initial injection stage and the breakthrough moment, respectively. It should be noted that the gas exhibits a higher flow velocity, establishing itself as the boundary between the injected fluid and the oil. The gas wets the rock and penetrates the spaces between the circular grains. It is important to mention that we disregarded wettability and surface tension in this work, which means that such dynamics arise from the disparity in fluid flow velocities, which is related to their viscosity and density. Examining these two images, similarities with the GF case emerge as a portion of the oil remains near the reservoir walls, and the breakthrough occurs at a time closer to the GF case ($t = 0.7\,s$) rather than the WF case ($t = 1.4\,s$). Concerning the pathways explored, a balanced blend of GF and WF dynamics is observed.

Figure 8c illustrate the volume fractions at $t = 5\,s$ (close to the end time). It is evident that as time progresses, the oil initially left behind is gradually displaced. Notably, this figure shows an intriguing dynamic where the injected fluids explore alternative pathways, reminiscent of the GF case, but with enhanced efficiency due to the unique characteristics of both fluids.

In summary, the SWAG case combines the favorable aspects of both GF and WF scenarios, leading to a higher oil recovery. The gas, with its higher flow velocity, advances ahead of the water, exploring alternative regions. Simultaneously, the water follows the preferential path created, efficiently displacing the remaining oil near the reservoir walls.

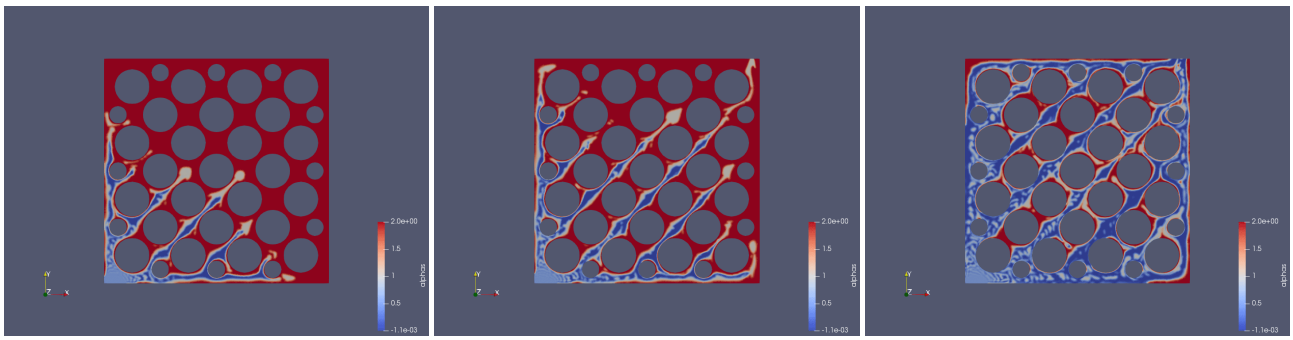

(a) Close to the start time, at $t = 0.5\,s$. (b) Before breakthrough, at $t = 0.85\,s$. (c) Close to the end time, at $t = 5.0\,s$.

Figure 8: Ternary saturation at different times during the simulation for the SWAG case. The water phase volume fraction is depicted in blue, the gas phase in gray and the oil phase is represented in red.

The results discussed in the previous paragraphs are presented in Figure 9, which shows the oil recovery factor (ORF) for all the cases examined. In WAG scenarios, the higher the proportion of injected water, the greater the final ORF. However, SWAG stands out by combining rapid oil production, at the beginning of the simulation, with sustained superiority throughout all time intervals, achieving the highest ORF among all the cases studied. Following closely behind are the WF, WAG 4:1, and WAG 3:1 cases, which exhibit similar ORFs. Notably, the curve for the SWAG case appears to exhibit a positive trend, suggesting that given more time, its ORF would continue to increase, in contrast to the observed trends in the other cases.

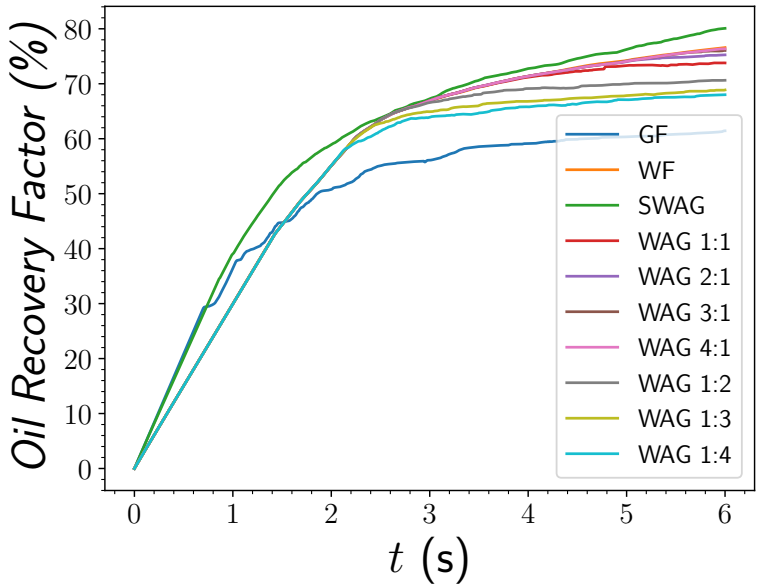


Figure 9: Comparison of Oil Recovery Factor (ORF) for GF, WF, SWAG and one cycle WAG with different ratios.

Table 1 displays the ORF values for the studied cases at $t = 1\,s$, $t = 2\,s$, $t = 3\,s$ and $t = 6\,s$. At $t = 1\,s$, all cases, except for those involving gas injection (GF and SWAG), exhibit the same ORF as they start with water injection. At this time, the GF and SWAG cases demonstrate ORFs that are respectively $21.44\%$ and $30.14\%$ higher than WAG/GF cases.

Moving to $t = 2\,s$, the GF case shows the lowest ORF, in contrast to the previous time point where it ranked second. This can be attributed to the gas dynamics, which, despite flowing at a high speed, leaves a significant portion of oil behind. In the WAG/WF cases, minimal differences of less than $0.1\%$ are observed. Meanwhile, the SWAG case maintains the highest ORF, surpassing the WAG/GF cases by $6.97\%$.

Table 1: Comparison of Oil Recovery Factor for one cycle WAG with different ratios.

| Case | Oil Recovery Factor [%] | | | |
|---|---|---|---|---|
| | t = 1s | t = 2s | t = 3s | t = 6s |
| GF | 36.42 | 50.77 | 56.08 | 61.44 |
| WF | 29.99 | 55.10 | 66.93 | 76.59 |
| SWAG | 39.03 | 58.94 | 67.27 | 80.08 |
| WAG 1:1 | 29.99 | 55.10 | 66.92 | 73.79 |
| WAG 2:1 | 29.99 | 55.10 | 66.93 | 75.26 |
| WAG 3:1 | 29.99 | 55.10 | 66.93 | 76.06 |
| WAG 4:1 | 29.99 | 55.10 | 66.93 | 76.36 |
| WAG 1:2 | 29.99 | 55.10 | 66.58 | 70.63 |
| WAG 1:3 | 29.99 | 55.11 | 64.92 | 68.87 |
| WAG 1:4 | 29.99 | 55.14 | 63.89 | 68.01 |

At $t = 3\,s$, the difference between the WAG/WF cases increases to $4.76\%$ due to the switch to gas injection in certain WAG schedules. It is noteworthy that the cases with gas injection in WAG cases experience a decrease in ORF. Additionally, the GF case remains at the lowest ORF, while the SWAG case continues to lead with a slight improvement of $0.51\%$ compared to the second-ranked WF case.

Finally, at the final time point of the simulation ($t = 6\,s$), the SWAG case claims first place with an ORF $4.56\%$ higher

than the second-ranked WF case, which, in turn, exhibits an ORF 0.30% higher than the third-placed WAG 4:1 case. The GF case occupies the last position with an ORF 23.28% lower than that of the SWAG case.

As previously discussed, the injection of different fluids, in different proportions and schedules, into the reservoir results in different fluid dynamics. To better understand the outcome of the winning schedules, Figure 10 depicts the ternary saturation for the top three placements (SWAG, WF, and WAG 4:1), as well as the last placement (GF), at the final simulation time ($t = 6\,s$).

Figures 10a and 10b display the final time for the GF and WF cases, respectively, revealing that even after the entire simulation period, both schedules failed to overcome their negative aspects. In this regard, the GF case leaves a significant amount of oil behind, particularly around the grains, but manages to explore alternative paths in the reservoir. On the other hand, the WF case effectively sweeps the reservoir in regions where the injected fluid comes into contact with the oil but falls short in exploring alternative pathways, especially evident in the central region of the reservoir.

Figure 10c illustrates the results for the WAG 4:1 case, where it can be observed that despite the alternation of both fluids, the positive aspects of both schedules (GF and WF) are subtly merged. It is noticeable that the remaining oil in the areas close to the inlet is minimal, making it more efficient than the GF case, but slightly less efficient than the WF case in this aspect. However, in the central regions of the reservoir, there is a certain tendency for the injected fluid to seek new paths, although not as clearly demonstrated as in the SWAG case.

Figure 10d shows the Ternary Saturation of the SWAG case at the end of the simulation ($t = 6\,s$). Here, the positive aspects of both schedules (GF and WF) are combined. All the oil around the grains adjacent to the inlet is completely swept away, similar to the WF case. Moreover, a significant portion of the alternative pathways in the central region is explored, resembling the behavior observed in the GF case. The combination of these two advantages justifies the higher ORF of the SWAG case compared to the other cases studied.

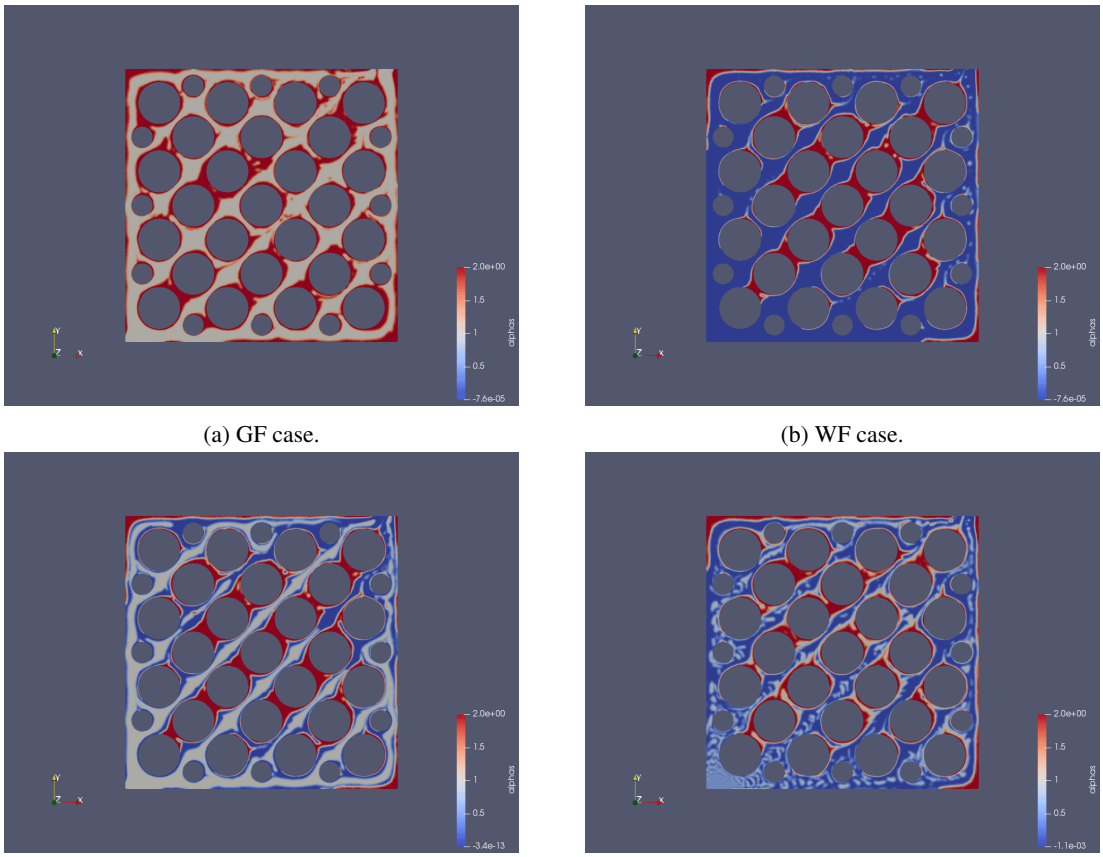

(a) GF case.

(b) WF case.

(c) WAG 4:1 case.

(d) SWAG case.

Figure 10: Ternary Saturation at $t = 6\,s$ for GF, WF, WAG 1:4 and SWAG. The water phase volume fraction is depicted in blue, the gas phase in gray and the oil phase is represented by the red color.

Figure 11 presents a summary of the results obtained for the SWAG case. The figure depicts the growth of the Oil Recovery Factor (ORF) over time, along with the Ternary Saturation of the SWAG case at various time intervals. Throughout the evaluated period, it is evident that there is a consistent tendency to explore different pathways. Initially, this sweeping action leaves some oil behind, as it is primarily driven by the gas phase. However, as time progresses, more and more oil is removed from these regions with the arrival of the water phase. Consequently, in the final moments of

the simulation, a substantial amount of oil has been extracted from the interstitial spaces between the grains in the central region of the reservoir.

To summarize the previous results, we observe that the gas phase is responsible for exploring different regions of the reservoir, while the water phase effectively removes the remaining oil from these regions. The presence of areas where only the gas has swept the oil at the end of the simulation suggests that if the simulation time were extended, the water phase would reach these pores, further enhancing the sweeping efficiency in this region and resulting in a larger ORF. It is important to emphasize that this study is preliminary, and certain simplifications were employed to address the complexity of the problem.

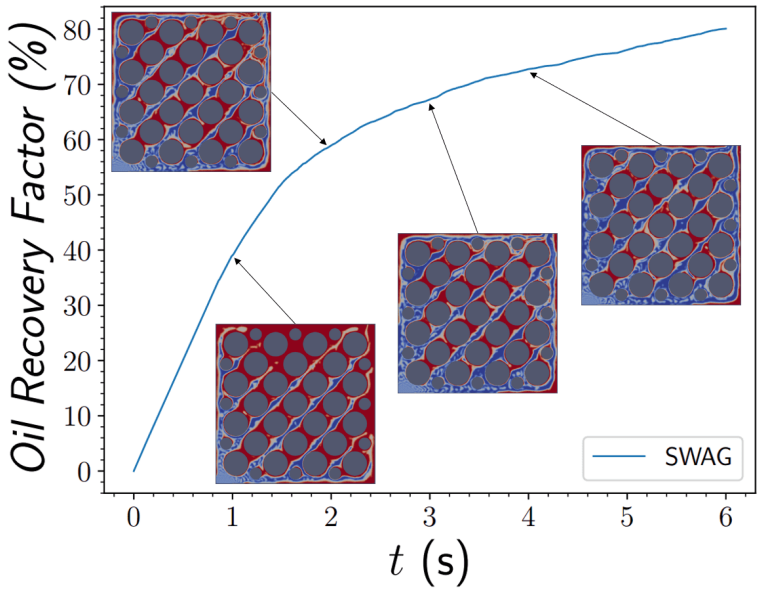


Figure 11: Oil Recovery Factor with Ternary Saturation for SWAG case.

## 4. Conclusion

The present study investigated of the impact of different injection schedules, including the traditional WF and GF, as well as WAG with various ratios and SWAG, on the Oil Recovery Factor in a synthetic domain with high porosity. The fluid properties used in the simulations were similar to those found in pre-Brazilian salt formations. It is important to acknowledge that this study represents a preliminary explorations and some simplifications were employed, such as neglecting surface tension, wettability effects and compressibility. Despite these simplifications, the findings of this study provide some insights into the effects of injection schedules on oil recovery in porous media.

The results demonstrated that the SWAG case achieved the highest ORF compared to the other injection schedules, with a significant improvement of $4.56\%$ over the second-place WF case. Among the WAG cases examined, it was observed that increasing the proportion of water led to higher ORF values at the end of the simulation. This can be attributed to the distinct characteristics of the two fluids in the simplified model. The gas phase, with its high velocity, effectively explored regions of the reservoir that water alone could not reach. On the other hand, the water phase demonstrated superior sweeping capabilities, leaving no residual oil behind.

The SWAG injection strategy successfully combined the advantages of GF and WF, effectively removing oil from regions close to the grains while also exploring areas that were not accessible to the WF case. In this case, the gas phase played a vital role in exploring different regions of the reservoir, while the water phase efficiently swept away the remaining oil from these regions.

Our results demonstrate that cases involving initial gas injection lead to enhanced oil production during the initial simulation period. In future works, we intend to investigate the WAG injection approach starting with gas, while also incorporating wettability and surface tension effects into the numerical methodology. Furthermore, our plans include utilizing domains that closely resemble real field conditions, encompassing irregular grains, intricate pathways, and reduced porosity.

## 5. ACKNOWLEDGEMENTS

The authors gratefully acknowledge the support provided by Repsol Sinopec Brasil and ANP (National Agency of Petroleum, Natural Gas, and Biofuels) for the present study, under ANP Project No. 22675-3, as well as the support from CAPES (Coordination for the Improvement of Higher Education Personnel).

## 6. REFERENCES

Afzali, S., Rezaei, N. and Zendehboudi, S., 2018. "A comprehensive review on enhanced oil recovery by water alternating gas (WAG) injection". *Fuel*, Vol. 227, pp. 218–246.

Al-Khulaifi, Y., Lin, Q., Blunt, M.J. and Bijeljic, B., 2019. "Pore-scale dissolution by CO2 saturated brine in a multimineral carbonate at reservoir conditions: Impact of physical and chemical heterogeneity". *Water Resources Research*, Vol. 55, No. 4, pp. 3171–3193.

Al-Shuraiqi, H.S., 2005. *Mechanisms of oil recovery via first contact miscible WAG injection*. Ph.D. thesis, Imperial College London.

Blunt, M.J., Bijeljic, B., Dong, H., Gharbi, O., Iglauer, S., Mostaghimi, P., Paluszny, A. and Pentland, C., 2013. "Pore-scale imaging and modelling". *Advances in Water resources*, Vol. 51, pp. 197–216.

Britto, A., Vivas, C., Almeida, M., da Cunha Lima, I. and da Cunha Lima, A., 2020. "Multiphase flow mobility impact on oil reservoir recovery: An open-source simulation". *AIP Advances*, Vol. 10, No. 3, p. 035032.

Christensen, J.R., Stenby, E.H. and Skauge, A., 2001. "Review of WAG field experience". *SPE Reservoir Evaluation & Engineering*, Vol. 4, No. 02, pp. 97–106.

Christie, M., Muggeridge, A., Barley, J. *et al.*, 1993. "3D simulation of viscous fingering and WAG schemes". *SPE Reservoir Engineering*, Vol. 8, No. 01, pp. 19–26.

de Freitas, V.R., Fortaleza, E.L.F., Limaverde Filho, J.O.D.A. and Munerato, F.P., 2020. "COB-2021-2104 Analysis of Water Alternating Gas (WAG) in an Immiscible Reservoir". In *Proceedings of the 26th ABCM International Congress of Mechanical Engineering, Virtual Conference, Brazil*. ABCM, pp. 3–8.

Fabian, N., Moreland, K., Thompson, D., Bauer, A.C., Marion, P., Gevecik, B., Rasquin, M. and Jansen, K.E., 2011. "The paraview coprocessing library: A scalable, general purpose in situ visualization library". In *2011 IEEE Symposium on Large Data Analysis and Visualization*. IEEE, pp. 89–96.

Fortaleza, E.L.F., Neto, E.P.B. and Miranda, M.E.R., 2020. "Production optimization using a modified net present value". *Computational Geosciences*, Vol. 24, pp. 1087–1100.

Geuzaine, C. and Remacle, J.F., 2009. "Gmsh: A 3-d finite element mesh generator with built-in pre-and post-processing facilities". *International journal for numerical methods in engineering*, Vol. 79, No. 11, pp. 1309–1331.

Guédon, G.R., Inzoli, F., Riva, M. and Guadagnini, A., 2019. "Pore-scale velocities in three-dimensional porous materials with trapped immiscible fluid". *Physical Review E*, Vol. 100, No. 4, p. 043101.

Iyi, D., Balogun, Y., Oyeneyin, B. and Faisal, N., 2021. "Numerical modelling of the effect of wettability, interfacial tension and temperature on oil recovery at pore-scale level". *Journal of petroleum science and engineering*, Vol. 201, p. 108453.

Ju, Y., Gong, W., Chang, W. and Sun, M., 2020. "Effects of pore characteristics on water-oil two-phase displacement in non-homogeneous pore structures: A pore-scale lattice boltzmann model considering various fluid density ratios". *International Journal of Engineering Science*, Vol. 154, p. 103343.

Menke, H.P., Bijeljic, B., Andrew, M.G. and Blunt, M.J., 2015. "Dynamic three-dimensional pore-scale imaging of reaction in a carbonate at reservoir conditions". *Environmental science & technology*, Vol. 49, No. 7, pp. 4407–4414.

Mousavi Mirkalaei, S.M., Hosseini, S.J., Masoudi, R., Ataei, A., Demiral, B.M. and Karkooti, H., 2011. "Investigation of different I-WAG schemes toward optimization of displacement efficiency". In *SPE Enhanced Oil Recovery Conference*. OnePetro.

Raeini, A.Q., Blunt, M.J. and Bijeljic, B., 2012. "Modelling two-phase flow in porous media at the pore scale using the volume-of-fluid method". *Journal of Computational Physics*, Vol. 231, No. 17, pp. 5653–5668.

Ramachandran, K.P., Gyani, O.N. and Sur, S., 2010. "Immiscible hydrocarbon WAG: laboratory to field". In *SPE oil and gas India conference and exhibition*. OnePetro.

Ranaee, E., Guédon, G.R., Moghadasi, L., Inzoli, F., Riva, M., Maddinelli, G., Bartosek, M. and Guadagnini, A., 2020. "Implementation of three-phase black-oil reservoir models assisted by micro-scale analyses". In *SPE Europec*. OnePetro.

Skauge, A. and Stensen, J.Å., 2003. "Review of WAG field experience". In *Oil Recovery–2003, 1st International Conference and Exhibition, Modern Challenges in Oil Recovery*. pp. 19–23.

Yu, T., Li, B., Hao, M. and Song, B., 2022. "Study on microscopic water flooding in porous carbonate reservoirs by numerical simulation". *Geofluids*, Vol. 2022.

Zhao, J. and Wen, D., 2017. "Pore-scale simulation of wettability and interfacial tension effects on flooding process for enhanced oil recovery". *RSC advances*, Vol. 7, No. 66, pp. 41391–41398.

Zhu, G., Yao, J., Li, A., Sun, H. and Zhang, L., 2017. "Pore-scale investigation of carbon dioxide-enhanced oil recovery". *Energy & Fuels*, Vol. 31, No. 5, pp. 5324–5332.

## 7. RESPONSIBILITY NOTICE

The authors are solely responsible for the printed material included in this paper.